Contents lists available at ScienceDirect

Cell Calcium

Ca²⁺ images obtained in different experimental conditions shed light on the spatial distribution of IP₃ receptors that underlie Ca²⁺ puffs

Estefanía Piegari *, Lorena Sigaut, Silvina Ponce Dawson

Departamento de Física and IFIBA, CONICET, FCEyN-UBA, Ciudad Universitaria, Pabellón I, 1428 Buenos Aires, Argentina

ABSTRACT

Many intracellular Ca²⁺ signals involve Ca²⁺ release from the endoplasmic reticulum through inositol 1,4,5-trisphosphate receptors (IP₃Rs). The open probability of IP₃Rs depends on cytosolic Ca²⁺ so that these signals involve Ca²⁺-induced Ca²⁺-release (CICR). IP₃Rs are organized in clusters. The signals they mediate are observed using single-wavelength dyes and, often, a slow Ca²⁺ buffer (EGTA) is added to disrupt CICR between clusters and keep the signals spatially restricted. It is assumed that the presence of the dye or of EGTA does not alter the intra-cluster Ca²⁺ dynamics. In this paper we analyze this issue combining experiments and numerical simulations. We compare the properties of local signals known as *puffs* observed with different dyes and EGTA concentrations. We determine that although the dye or EGTA does not alter the intra-cluster dynamics, the set of observable events is different depending on the degree of inter-cluster uncoupling of the experiment. An analysis of the observations shows that the events that are missed for insufficient inter-cluster uncoupling are those of fastest amplitude growth rate. This agrees with a spatial organization in which the largest amplitude events correspond to clusters with densely packed active IP₃Rs.

© 2015 Elsevier Ltd. All rights reserved.

1. Introduction

Calcium (Ca²⁺) signals are ubiquitous and their versatility relies on the variety of spatio-temporal behaviors that the intracellular Ca²⁺ concentration can display. Intracellular signals usually involve Ca²⁺ release from internal stores through channels that open more or less frequently depending on the amount of cytosolic Ca²⁺ [1,2]. Inositol 1,4,5-trisphosphate receptors (IP₃Rs) are the primary cytosolic target for the initiation of intracellular Ca²⁺ signals [3]. IP₃Rs need to bind IP₃ and Ca²⁺ to become open [2]. This last feature is responsible for the occurrence of calcium induced calcium release (CICR). In most cells IP₃Rs are organized in clusters. The signals remain localized (i.e., involving the release through one or more IP₃Rs in a cluster) or global depending on the efficiency of the released Ca²⁺ to elicit the opening of IP₃Rs from many clusters. Localized signals in which Ca²⁺ is released from the endoplasmic reticulum through IP₃Rs that belong to a single channel cluster are known as *puffs* [2]. They are the building blocks of more global

signals that propagate throughout the cell [4]. Obtaining a detailed characterization of *puffs* is thus of great interest.

Ca²⁺ puffs are observed using Ca²⁺ dyes and different optical techniques. Ca²⁺ fluorophores need to bind Ca²⁺ to change their fluorescence properties [5]. Thus, the observed fluorescence is related to the Ca²⁺-bound dye concentration, which depends on the ability of the dye to overcome the various Ca²⁺ trapping mechanisms of the cell. This binding by the dye also affects the signals themselves since it can alter CICR. Furthermore, to study the kinetics of puffs a slow exogenous Ca²⁺ buffer that disrupt inter-cluster coupling (typically, EGTA) is added in many experiments [4]. Because of the slow EGTA kinetics it is assumed that its addition does not alter CICR at the intra-cluster level or compete with the dye for Ca²⁺ during a localized signal so that neither the underlying Ca²⁺ dynamics nor the fluorescence distribution is affected by EGTA [4].

In this paper we study to what extent experiments performed with different dyes and/or [EGTA] are able to detect Ca²⁺ puffs with similar accuracy and in which ways the different experimental conditions affect the observed puff properties and the underlying dynamics of Ca²⁺ itself. To this end we combine numerical simulations and experiments performed in *Xenopus laevis* oocytes using EGTA and single wavelength Ca²⁺ dyes of different kinetics, Fluo-4 and Rhod-2. We use our classification method [6] to choose the combination of dye and EGTA concentrations that should report the occurrence of the same underlying Ca²⁺ signal with a similar

* Corresponding author at: Departamento de Física, Facultad de Ciencias Exactas y Naturales, UBA, Ciudad Universitaria, Pabellón I, 1428 Buenos Aires, Argentina. Tel.: +54 11 4576 3353; fax: +54 11 4576 3357.

E-mail address: estefipiegari@df.uba.ar (E. Piegari).

signal-to-noise ratio. We then repeat the experiments using Fluo-4 and different EGTA concentrations. The quantitative comparison of the puff properties distributions obtained for the various combinations probed shows that, even if they are equally able to report the occurrence of Ca^{2+} puffs, the set of observed events differs due to their different ability to disrupt inter-cluster communication. The puffs that are not elicited with the slowest dye or with the smallest EGTA concentrations show a rapid fluorescence growth. These "missing" events correspond to signals with very efficient intra-cluster CICR. This reveals that the largest amplitude puffs come from clusters with closely packed open IP_3Rs and shows that experiments performed under different conditions shed light on the spatial organization that underlies the observations. The experiments and numerical simulations also show that the fluorescence amplitude is nonlinearly related to the underlying increment in free Ca^{2+} even if the dye is not saturated as previously observed in [7,8].

2. Materials and methods

2.1. Experiments

2.1.1. Preparation of X. laevis oocytes

Experiments were performed on immature *X. laevis* oocytes previously treated with collagenase and stored in Barth's solution (composition in mM: NaCl, 88; KCl, 1; $CaCl_2 \cdot 2H_2O$, 0.41; $NaHCO_3$, 2.4; $MgSO_4 \cdot 7H_2O$, 0.82; $Ca(NO_3)_2 \cdot 4H_2O$, 0.33; HEPES, 5; containing 0.5 mg/ml gentamicin).

Intracellular microinjections were performed using a Drummond microinjector. Oocytes were loaded with either Fluo-4 dextran high affinity ($K_d = 772$ nM) or Rhod-2 ($K_d = 2000$ nM), together with caged IP_3 to induce channel opening and an exogenous Ca^{2+} buffer, EGTA, to vary the observed signals.

Assuming a 1 μl cytosolic volume, the final concentrations of Fluo-4, Rhod-2 and IP_3 were 36 μM, 90 μM and 9 μM, respectively. The final concentration of EGTA was varied between 45 μM and 300 μM for the experiments performed with Fluo-4, and was kept fixed at 45 μM for those performed with Rhod-2 (see Table 1).

2.1.2. Microscopy technique

Experiments were performed using an inverted microscope IX81 connected to a multispectral confocal unit Olympus FluoView 1000 in the linescan mode. The recording was done focusing with a 60× oil immersion objective (NA = 1.35) and imaging in the animal hemisphere of the oocytes bathed in normal Ringer's solution (composition in mM: NaCl, 120; KCl, 2; $CaCl_2 \cdot 2H_2O$, 1.8; HEPES, 5). The dyes Fluo-4 and Rhod-2 were excited with the 488 nm line of a multiline Argon laser and with the 543 nm line of a He–Ne laser, respectively. The emission was detected in the range of (500–600) nm for Fluo-4 and (555–655) nm for Rhod-2 with a PMT. Caged-IP_3 was photoreleased illuminating with the (350–400) nm region of the spectrum of a Hg lamp using the modification described in [9].

2.2. Image acquisition, processing and analysis

Linescan images were obtained by scanning along a fixed line (250 pixels) within the oocyte (10–15) μm. Different amounts of

Table 1
Combinations of dye and EGTA concentrations that were used in the experiments discussed in this paper.

Experiment label	Dye type and concentration	[EGTA] (μm)
Type I	[Fluo4] = 36 μM	90
Type II	[Fluo4] = 36 μM	300
Type III	[Rhod2] = 90 μM	45

caged IP_3 were photoreleased by photolysis flashes of variable duration. The acquisition was performed with a pixel time of 10 μs and a scan rate of 3.62 μs per line. In the images displayed, the distance along the scan line runs vertically and time runs from left to right. A typical linescan image is illustrated in Fig. 1A. In this figure, fluorescence of the calcium dye (in this case, Fluo-4) is shown at each point, x_i, along the linescan and time, t_j, as the ratio:

$$\Delta F_R(x_i, t_j) = \frac{F(x_i, t_j) - F_0(x_i)}{F_0(x_i)} \tag{1}$$

where $F_0(x_i)$ is the fluorescence at spatial point, x_i, averaged over time before the photolysis (UV) flash. Increasing levels of fluorescence are represented by increasingly warmer colors. The arrow in the figure marks the occurrence of the UV pulse. The bright fringes of the image correspond to the cytosol and the dark fringes to cortical granules.

2.2.1. Puff characterization

In order to identify and characterize puffs, the fluorescence, F, at each pixel of the image is averaged with the values at its eight nearest neighbors. From now on when we refer to the fluorescence of the image, F, we actually refer to this smoothed out. The ratio, ΔF_R, is also computed from these smoothed-out figures when needed.

Puffs are identified by visual inspection as a connected set of at least ∼20 pixels where F is sufficiently above the basal level. A rectangular region of the image that encloses the puff is then selected. The center of the puff is determined by the spatial location, x_c, and time, t_c, of the pixel at which ΔF_R is maximal over the selected region as shown in Fig. 1B.

In order to determine the amplitude and temporal parameters of the observed event, we compute $\langle \Delta F_R \rangle_x(t)$ by averaging $\Delta F_R(x, t)$ over eleven horizontal lines (the line that corresponds to $x = x_c$ and five below and five above it). The rise time, decay time and amplitude are subsequently computed as illustrated in Fig. 1C. The amplitude, A, is defined as the maximum over time, $A \equiv \max_t \langle \Delta F_R \rangle_x(t)$. Denoting t_{amp} as the time, t, at which $\langle \Delta F_R \rangle_x(t) = \langle \Delta F_R \rangle_{x,\max}$, the beginning of the puff is identified by t_{start} the largest time, t, that satisfies $t < t_{amp}$ and $\langle \Delta F_R \rangle_x(t) = 0.1 \langle \Delta F_R \rangle_{x,\max}$. The end of the puff is identified by t_{end}, the smallest time, t, that satisfies $t > t_{amp}$ and $\langle \Delta F_R \rangle_x(t) = 0.1 \langle \Delta F_R \rangle_{x,\max}$. The rise time, decay time, and duration of the puff are then defined as $t_R \equiv t_{amp} - t_{start}$, $t_D \equiv t_{end} - t_{amp}$ and $t_{end} - t_{start}$, respectively. We also compute the amplitude growth rate as $GR = 0.9A/t_R$.

In order to determine the parameters that characterize the spatial spread of the observed event we first compute the mean, m, and standard deviation, σ, of ΔF_R over the bright fringes of the whole image. We then compute threshold $= m + \sigma + 0.2 * (A - m - \sigma)$ for each puff of the image and $\langle \Delta F_R \rangle_t(x)$ by averaging F over five vertical lines (the one that corresponds to $t = t_c$ and two to the left and two to the right of it). We identify the points x_i in the selected region that satisfy $\langle \Delta F_R \rangle_t(x_i) > $ threshold, define $x_{\min} = \min_i \{x_i\}$ and $x_{\max} = \max_i \{x_i\}$ and, from them, width $= x_{\max} - x_{\min}$. We illustrate the procedure in Fig. 1D.
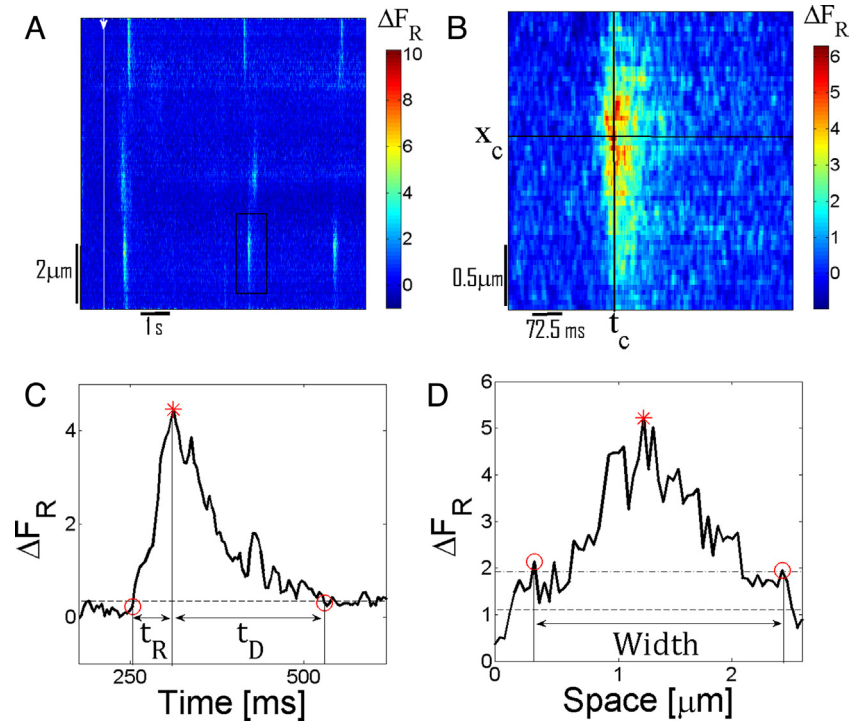
2.2.2. Statistical analysis

To analyze the experimental results we calculate the histograms of the parameters obtained expressing them in terms of frequency of occurrence, $N(X)/N_{total}$, where $N(X)$ is the number of puffs with X in a given bin and N_{total} is the total number of analyzed puffs. We use a uniform bin size, h, so that $N(X)/N_{total} = hf(X)$ with f the probability density function of X. The number of bins is $k = \Delta X/h$ with ΔX the range of obtained values and the bin size is chosen as $h = 2r/N_{total}^{1/3}$, where r is the distance, $r = X_{3/4} - X_{1/4}$, between the values, $X_{1/4}$ and $X_{3/4}$, that correspond to the first and third quartiles, respectively,

Fig. 1. Linescan images and puff characterization. (A) Representative linescan image obtained with Fluo-4, acquired with a pixel time of 10 μs and a scan rate of 3.62 ms per line. Puffs were evoked by a photolysis flash at the time marked by the arrow. (B) Spatiotemporal distribution of F_R from the puff surrounded by the black box in (A). The center of the puff is identified by the spatial and temporal coordinates, x_c and t_c, respectively. (C) Temporal profile obtained from the image in (B) by averaging eleven horizontal lines around x_c. The quantities with which we characterize the puff amplitude and time course are indicated in the figure. (D) Spatial profile obtained from the image in (B) by averaging five vertical lines around t_c. The puff width is indicated in the figure.

of the cumulative density function (CDF), $F(X) = \int_0^X f(X')dX'$. To compare two distributions of the same parameter obtained under different experimental conditions, $F_1(X)$ and $F_2(X)$, we perform a Kolmogorov–Smirnov test. The test statistic is:

$$\max \left| F_1(X) - F_2(X) \right|, \tag{2}$$

where each $F_i(X)$ is the corresponding cumulative density function that we compute numerically as: $F_i(X) = \sum_{X' \leq X} N_i(X')/N_{i,\text{total}}$

2.3. Numerical simulations

2.3.1. Deterministic Ca²⁺-bound dye distribution in the presence of a single source

We perform numerical simulations of the Ca²⁺ dynamics in the cytosolic medium solving a set of reaction–diffusion equations in a spherical volume (assuming spherical symmetry) for Ca²⁺, an immobile endogenous buffer (S), a cytosolic Ca²⁺ indicator (D) and an exogenous mobile buffer (EGTA). In some cases we also consider an additional (mobile) buffer (M). A point Ca²⁺ source located at the origin and pumps (P) that remove Ca²⁺ uniformly in space are also included. The source represents a cluster of IP₃R's.

We consider that a single Ca²⁺ ion binds to a single buffer or dye molecule according to:

$$Ca^{2+} + X \underset{k_{\text{off}-X}}{\overset{k_{\text{on}-X}}{\rightleftarrows}} [CaX] \tag{3}$$
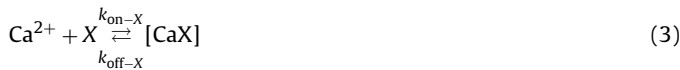
where X represents D, EGTA, S or M, and $k_{\text{on-}X}$ and $k_{\text{off-}X}$ are the forward and backward binding rate constants of the corresponding reaction, respectively. We assume that the total concentrations of dye, EGTA, mobile and immobile buffer remain constant ($[D]_T$, $[EGTA]_T$, $[M]_T$, and $[S]_T$, respectively) and that the diffusion coefficients of their free and Ca²⁺ bound forms are equal. Therefore we calculate the free concentrations, $[D]$, $[EGTA]$, $[M]$ and

$[S]$ by subtracting the concentration of their Ca²⁺ bound forms to their total concentrations. Given these assumptions, the set of reaction–diffusion equations reads:

$$\frac{\partial[Ca^{2+}]}{\partial t} = D_{Ca}\nabla^2[Ca^{2+}] - \sum_{X=D,S,M,EGTA} R_{CaX} + \text{source} \cdot \delta(r)$$

$$- [P]_T \frac{[Ca^{2+}]^2}{[Ca^{2+}]^2 + k_{\text{off}-T}} \tag{4.a}$$

$$\frac{\partial[CaD]}{\partial t} = D_{\text{dye}}\nabla^2[CaD] + R_{CaD} \tag{4.b}$$

$$\frac{\partial[CaEGTA]}{\partial t} = D_{EGTA}\nabla^2[CaEGTA] + R_{CaEGTA} \tag{4.c}$$

$$\frac{\partial[CaM]}{\partial t} = D_M\nabla^2[CaM] + R_{CaM} \tag{4.d}$$

$$\frac{\partial[CaS]}{\partial t} = R_{CaS} \tag{4.e}$$

where D_{Ca}, D_{dye}, D_M and D_{EGTA} are the diffusion coefficients of Ca²⁺, D, M and EGTA, respectively. The reaction terms, R_{CaX}, are derived from the kinetic scheme, Eq. (3).

$$R_{CaX} = k_{\text{on-}X}[Ca^{2+}]([X]_T - [CaX]) - k_{\text{off-}X}[CaX] \tag{5}$$

We assume no flux boundary conditions at $r = 20.5$ μm with r the radial coordinate. For the source we assume that it consists of $n_C = 10$ channels that open simultaneously at $t = 0$ each of which closes after a time that is drawn from an exponential distribution with mean t_{open} [10]. For the initial condition, we assume that all concentrations are homogeneously distributed, Ca²⁺ is at basal concentration and all species are in equilibrium among themselves ($R_{CaX} = 0$ for all X ($t = 0$)).

Table 2
Parameters values used to solve the simulations introduced in Section 2.4.

Parameter	Value	Units
Free calcium:		
D_{Ca}	220	$\mu m^2 s^{-1}$
$[Ca^{2+}]_{basal}$	0.1–0.3	μM
Calcium dye Fluo4-dextran:		
D_{dye}	15	$\mu m^2 s^{-1}$
k_{on-D}	240	$\mu M^{-1} s^{-1}$
k_{off-D}	180	s^{-1}
$[D]_T$	36	μM
Calcium dye Rhod2-dextran:		
D_{dye}	15	$\mu m^2 s^{-1}$
k_{on-D}	70, 85	$\mu M^{-1} s^{-1}$
k_{off-D}	130, 170	s^{-1}
$[D]_T$	36, 90	μM
Exogenous buffer EGTA:		
D_{EGTA}	80	$\mu m^2 s^{-1}$
$k_{on-EGTA}$	5	$\mu M^{-1} s^{-1}$
$k_{off-EGTA}$	0.75	s^{-1}
$[EGTA]_T$	45, 90	μM
Endogenous immobile buffer:		
K_{on-I}	400	$\mu M^{-1} s^{-1}$
K_{off-I}	800	s^{-1}
$[I]_T$	300	μM
Slow endogenous mobile buffer:		
D_M	27	$\mu m^2 s^{-1}$
K_{on-M}	20	$\mu M^{-1} s^{-1}$
K_{off-M}	8.6	s^{-1}
$[M]_T$	250	μM
Rapid endogenous mobile buffer:		
D_M	32	$\mu m^2 s^{-1}$
K_{on-M}	500	$\mu M^{-1} s^{-1}$
K_{off-M}	750	s^{-1}
$[M]_T$	10	μM
Pump:		
K_{off-P}	0.1	s^{-1}
$[M]_T$	0.9	μM
Source:		
n_c	10	
t_{open}	20	ms

The reaction–diffusion equations are solved using a backward Euler method in time and an explicit finite-difference formula in space with a 2nd order expression (first neighbors) for the Laplacian. The spatial grid size is $dr = 0.041\,\mu m$ and the time step $dt = 10\,\mu s$. The values of the parameters (taken from [11]) used in the simulations are listed in Table 2. To compare with experimental confocal signals we calculate a weighted average of [CaD] along the linescan $\boldsymbol{r} = (x, 0, 0)$ according to the confocal microscope point spread function (PSF). In this case, following [12]:

$$[\overline{CaD}](x, t) = \frac{\int [CaD](\boldsymbol{r}', t) \times \exp(-2((x - x')^2 + y'^2)/w_r^2 - 2z'^2/w_z^2)dx'dy'dz'}{V} \quad (6)$$

where $w_r = 0.23\,\mu m$, $w_z = 1.15\,\mu m$ and $V = w_r^2 w_z (\pi/2)^{3/2}$. This is this blurred version of the Ca^{2+}-bound dye concentration.

In order to compare the Ca^{2+}-bound dye distribution obtained in simulations that mimic the conditions of Type I, Type II and Type III experiments in the presence of the same point source we compute the relative increment in $\overline{CaD}$:

$$\Delta[CaD]_R = \frac{[\overline{CaD}] - [\overline{CaD}]_b}{[\overline{CaD}]_b} \quad (7)$$

where $[\overline{CaD}]$ is computed as in Eq. (6) and $[\overline{CaD}]_b$ is the Ca^{2+}-bound dye concentration at basal conditions. The amplitude of the signal is defined as:

$$A = \max_t \left(\frac{\Delta[\overline{CaD}]}{[\overline{CaD}]_b(0, t)} \right) \quad (8)$$

The decay time of the signal in the Ca^{2+}-bound dye distribution is computed from the temporal profile of $\Delta[\overline{CaD}]/[\overline{CaD}]_b$ at the origin (the site of Ca^{2+} release) as the time, t_D, such that $\Delta[\overline{CaD}]/[\overline{CaD}]_b(0, t_D) = 0.1A$. The width is computed from the spatial profile of $\Delta[\overline{CaD}]/[\overline{CaD}]_b(x, t_{max})$ with t_{max} the time at which $\Delta[\overline{CaD}]/[\overline{CaD}]_b(0, t)$ is maximum as twice the value of x such that $\Delta[\overline{CaD}]/[\overline{CaD}]_b(x, t_{max}) = 0.5A$.

To assess the rate of CICR-mediated coupling between neighboring clusters we compute the probability that an IP$_3$R located at a distance, d, from a source that is releasing Ca^{2+} opens during an interval, Δt, since the start of the release by means of:

$$P_O(d, \Delta t) = 1 - \exp\left(-\int_0^{\Delta t} k_{on}[Ca^{2+}](d, t)dt \right) \quad (9)$$

with $k_{on} = 20\,\mu M^{-1} s^{-1}$ the rate of Ca^{2+} binding to the activating site of an IP$_3$R of the DeYoung–Keizer model [10].

2.3.2. Numerically simulated fluorescence distribution

In order to generate noisy simulated images from the simulations described in Section 2.3.1 we follow the method described in [6]. Briefly, for each position, x, and time, t, of the simulation, we draw a stochastic variable, $N(x, t)$, from a Poisson distribution of mean $\langle N \rangle$. We then compute the fluorescence at each pixel, $F(x, t)$, according to:

$$F = \gamma \text{Poisson}((q_1 - q_2)\text{Binomial}(p, N) + q_2 N) \quad (10)$$

where $N = N(x, t)$ and $p = \frac{[\overline{CaD}](x, t)}{[D]_T}$ with $[\overline{CaD}](x, t)$ obtained from the simulations as defined in Eq. (6). Assuming that the ratio q_2/q_1 is approximately given by the ratio of quantum efficiencies of [13] ($q_2/q_1 = 0.025$ for Fluo-4 and $q_2/q_1 = 0.07$ for Rhod-2), the values of γ, q_1, q_2 and $\langle N \rangle$ were estimated from the fluctuation analysis of [6] $\gamma \cong 5$, $q_1 = 0.45$, $q_2 = 0.01$, $\langle N \rangle = 32$ for Type I experiments and $\gamma \cong 6$, $q_1 = 0.36$, $q_2 = 0.02$, $\langle N \rangle = 80$ for Type III experiments. Given the numerically generated image corresponding to a simulation with a Ca^{2+} point source, the decay time and puff width are calculated as with the experimental signals.

3. Results

3.1. The effect of EGTA on puff properties

3.1.1. Experiments: puffs with a faster fluorescence growth are observed for increasing [EGTA]

We show in Fig. 2A and B the rise-time, t_R, distribution obtained for Type I (A) and for Type II (B) experiments. The corresponding mean rise time, $\langle t_R \rangle$, and standard deviations, σ_{t_R}, are $\langle t_R \rangle = 126.1$ ms and $\sigma_{t_{rise}} = 129.9$ ms for Type I and $\langle t_R \rangle = 93.7$ ms and $\sigma_{t_{rise}} = 63.5$ ms for Type II experiments. Analogously, we show in Fig. 2C and D the amplitude distributions obtained for Type I (C) and for Type II (D) experiments. The corresponding mean amplitude, $\langle A \rangle$, and standard deviations, σ_A, are $\langle A \rangle = 1.8$ au and $\sigma_A = 0.9$ au for Type I and $\langle A \rangle = 1.5$ au and $\sigma_A = 0.7$ au for Type II. A direct comparison of the distributions with of a Kolmogorov test performed on the corresponding CDFs rejects the null hypothesis that the amplitudes come from the same continuous distribution with a 5% significance level ($p_{value} = 0.002$). Most previous experiments and numerical simulations, however, show that puff amplitudes are not altered by the presence of EGTA. The simulations presented in the Fig. S1 show
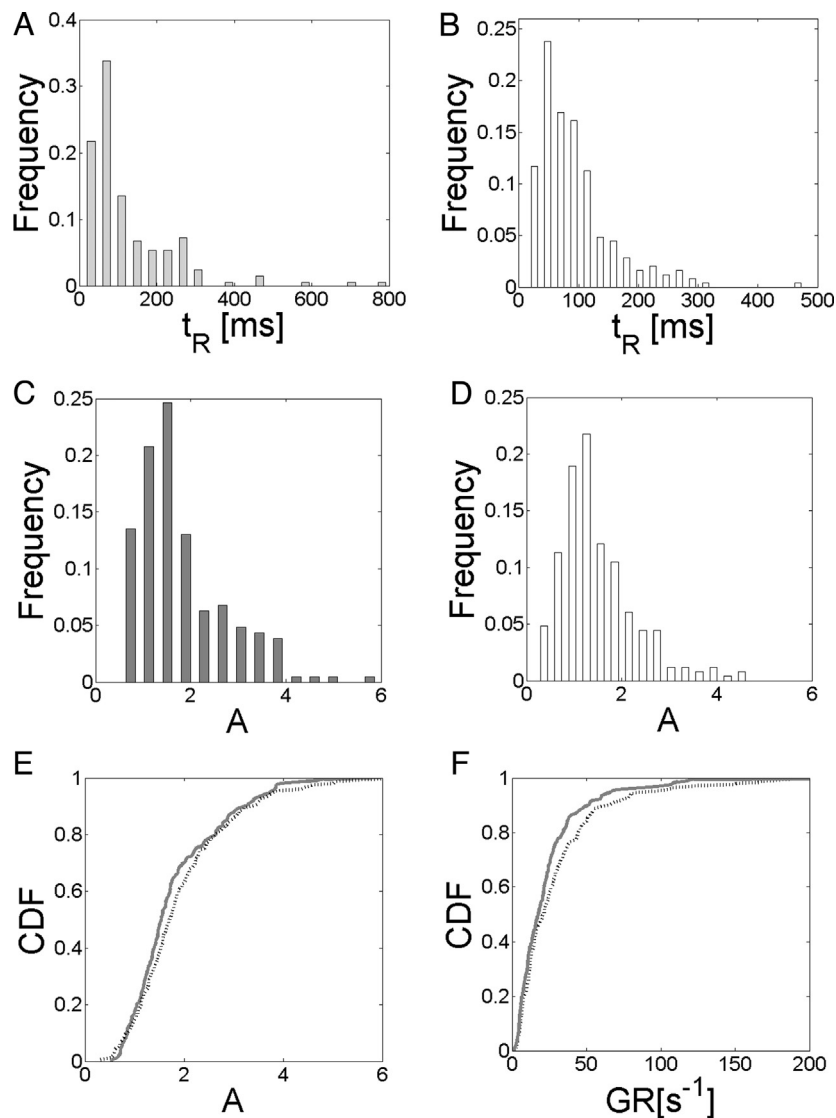
Fig. 2. Puff rise time, amplitude and amplitude growth rate distributions using Fluo4 and different EGTA concentrations. (A–D) Distributions obtained from $N = 207$ puffs observed in Type I (A, C) and from $N = 248$ puffs observed in Type II (B, D) experiments. The mean rise time and standard deviations are, respectively $\langle t_R \rangle = 126.1$ ms and $\sigma_{t_{rise}} = 129.9$ ms for Type I (A) and $\langle t_R \rangle = 93.7$ ms and $\sigma_{t_{rise}} = 63.5$ ms for Type II (B) experiments. The corresponding mean amplitude ($\langle A \rangle$) and standard deviations (σ_A) are $\langle A \rangle = 1.8$ au and $\sigma_A = 0.9$ au for Type I (C) and $\langle A \rangle = 1.5$ au and $\sigma_A = 0.7$ au for Type II (D). (E) Cumulative density function (CDF) of A for Type I (gray line) and of $1.3 * A$ for Type II experiments (dotted black line). (F) CDFs of GR (amplitude growth rate) obtained from Type I (gray line)) and from Type II (dotted black line) experiments. In the latter the growth rate was computed including the 1.3 amplitude conversion factor.

a slight decrease (3%) in puff amplitude in the presence of EGTA. This reduction in amplitude can account for part of the difference in the distributions of Fig. 2C and D. Changes in the absolute value of the amplitude could also arise due to changes in some experimental properties. In order to check whether the two distributions become similar if the amplitudes observed in one type of experiment is multiplied by a common factor, we compared the corresponding CDFs but multiplying all the amplitudes of Type II experiments by 1.3. In such a case the Kolmogorov test cannot reject the null hypothesis that the (rescaled) amplitudes come from the same continuous distribution with a 5% significance level ($p_{value} = 0.082$). This becomes apparent in Fig. 2E, where we show the CDF of A for Type I (gray line) and of $1.3 * A$ for Type II (dotted black line) experiments.

Supplementary Fig. S1 related to this article can be found, in the online version, at http://dx.doi.org/10.1016/j.ceca.2015.01.003.

Fig. 2A and B shows that, on average, the rise time of puffs observed with Type II experiments is smaller than of those observed in Type I experiments. The differences in the distributions are confirmed by the Kolmogorov test which rejects the hypothesis that

the data collected arise from the same continuous distribution $p_{value} = 0.029$. Fig. 2E shows that the amplitude distributions match when one of them is multiplied by a conversion factor. We now compare the rate at which the amplitude grows in both cases. Based on the results of Fig. 2E we do this using $1.3 * A$ in the case of Type II. We show the corresponding CDFs in Fig. 2F. The Kolmogorov test rejects the null hypothesis that the (rescaled) amplitudes growth rates come from the same continuous distribution with a 6.2% significance level ($p_{value} = 0.061$). Comparing the CDFs of the amplitude growth rate less than $100 \, s^{-1}$ for Type I with Type II experiments the Kolmogorov test cannot reject the null hypothesis that the (rescaled) amplitudes growth rates come from the same continuous distribution with a 5% significance level ($p_{value} = 0.528$).

3.1.2. Numerical simulations: the effect of varying [EGTA] on Ca^{2+} release from CaEGTA or CaDye and on intracluster IP_3R coupling

The comparison of Fig. 2F indicates that there are puffs that apparently are observed in Type II but not in Type I experiments that correspond to situations in which the amplitude grows very

fast. We analyzed whether this fast amplitude growth could be due to an additional Ca^{2+} release from Ca^{2+}-bound EGTA or Ca^{2+}-bound dye by means of numerical simulations (see Fig. S1). We observe that the net effect of EGTA and of the dye in the vicinity of the source is to trap Ca^{2+}. Therefore, the faster growth rate of the experiments observed in Type II but not in Type I experiments cannot be attributed to a release of Ca^{2+} from CaEGTA or CaFluo4 near the open channels. A net Ca^{2+} release occurs further away from the source. Furthermore, we observe a slight decrease (3%) in puff amplitude (i.e., in $\Delta[CaD]_R$ defined in Eq. (7)) when [EGTA] varies from 90 μM to 300 μM. Since the addition of EGTA could change $[Ca^{2+}]_{basal}$, we repeated the simulations using $[Ca^{2+}]_{basal} = 0.3\,\mu$M instead of 0.1 μM with no significant differences with respect to the case with $[Ca^{2+}]_{basal} = 0.1\,\mu$M (data not shown). We performed a series of experiments in oocytes to check if $[Ca^{2+}]_{basal}$ varied but did not obtain conclusive results. We also performed stochastic simulations to study if changing [EGTA] between 90 μM and 300 μM altered differently the intracellular IP$_3$R coupling. We found that it did not (see Fig. S2).

Supplementary Fig. S2 related to this article can be found, in the online version, at http://dx.doi.org/10.1016/j.ceca.2015.01.003.

3.2. Comparing puff properties observed with two dyes of different kinetics

The results of Section 3.1 indicate that the difference in amplitude growth rate observed in Type I and Type II experiments cannot be attributed to differences in the way that the underlying increase in free Ca^{2+} is reported by the Ca^{2+}-bound dye in each experimental type. It cannot be attributed either to changes in CICR at the intra-cluster level or to a release of Ca^{2+} from Ca^{2+} bound to EGTA or dye. There is always the possibility that a subset of events goes undetected because of differences in the signal-to-noise ratio between the two types of experiment. We have recently introduced a method to compare experimental settings in terms of the signal-to-noise ratio that can be expected when observing Ca^{2+} signals [6]. The application of this method to experiments performed with [Fluo4] or [Rhod2] allowed us to infer that the signal-to-noise ratio of Type I experiments should be similar to that of experiments performed with [Rhod2] = 90 μM and [EGTA] = 45 μM (Type III experiments, see Table 1). Not only [EGTA] is different between Type I and Type III experiments, but also the kinetics of the dye which can result in differences in the way in which each dye affects the dynamics of the signals. The previous analysis in terms of the signal-to-noise ratio [6] serves to discard the possibility that a subset of events be undetected due to noise when comparing puffs observed in Type I and in Type III experiments. In what follows we compare the properties of puffs extracted from 94 (10.25 μm × 10.86 s) images of Type I ([Fluo4] = 36 μM and [EGTA] = 90 μM) and 107 of Type III ([Rhod2] = 90 μM and [EGTA] = 45 μM) experiments where at least one puff was identified. From them we computed that, on average, 2.18 puffs/image were observed for Type I and 1.46 for Type III experiments. According to this calculation, it seems that Type I experiments are more efficient than those of Type III detecting puffs. In order to determine if this different ability depended on the type of puff that was observed, we repeated this calculation for puffs which amplitude was smaller than a certain value. We show the results obtained in Table 3. This table and the discussion of the following subsections show that it is the lack of large amplitude (and rapid growth rate) puffs in Type III experiments that is responsible for this apparent difference in puff detectability.

3.2.1. Puff amplitude, puff kinetics and puff width distributions

We show in Fig. 3A and B the puff rise time and the puff amplitude distributions for Type III experiments. Comparing the

Table 3

Average number of puffs within a certain amplitude range observed per image for experiments performed with Fluo-4 (Type I experiments) and Rhod-2 (Type III experiments).

Amplitude range	Type I experiments	Type III experiments
All amplitudes	2.18	1.46
$A < 3$	1.93	1.45
$A < 2.5$	1.72	1.44
$A < 2$	1.54	1.38
$A < 1.5$	1.04	1.17
$A < 1$	0.37	0.51

distributions of Fig. 3B with those of Fig. 2C we observe that both the mean puff amplitude and its standard deviation are larger for Type I than for Type III experiments. This agrees with the observation that the puffs of largest amplitude observed in Type I experiments are not observed in those of Type III (see Table 3). Comparing Figs. 2A and 3A we observe that $\langle t_R \rangle$ is slightly smaller in Type III than in Type I. This slight difference goes in the opposite direction for $\langle t_D \rangle$. Regarding puff width we observe that its mean width value is slightly different for both distributions ($\langle$Width$\rangle$ =1.1 μm for Type I and $\langle$Width$\rangle$ =1.3 μm for Type III) but the distributions themselves are not significantly different (see Fig. S3)

Supplementary Fig. S3 related to this article can be found, in the online version, at http://dx.doi.org/10.1016/j.ceca.2015.01.003.

Comparing the CDFs of the various parameters for Type I and Type III experiments we obtain that the Kolmogorov test cannot reject the null hypothesis that the rise (p_{value} = 0.292) and the decay time (p_{value} =0.547 see Fig. S3) come from the same continuous distribution with a 5% significance level. It does reject the corresponding hypothesis for the widths (see Fig. S3) and amplitudes. We show in Fig. 4 the CDFs of puff amplitude (A) and rise time (B) with gray (Type I) and black (Type III) curves. As for the case of Type I and Type II experiments, the first direct comparison of the various puff property distributions obtained for Type I and Type III experiments shows differences in the observed amplitudes. Although $\langle t_R \rangle$ is slightly smaller for Type III experiments, the difference in t_R is not significant as determined from the comparison of the CDFs.

3.2.2. Numerically generated realistic Ca^{2+} images

In order to study to what extent the different kinetics of Fluo-4 and Rhod-2 could affect differently the observed images we performed a series of numerical simulations. We first analyzed the (cytosolic) Ca^{2+}-bound dye distribution obtained with deterministic simulations as described in Section 2.3.1. We observed slightly larger amplitudes for Type III than for Type I experiments in the presence of the same source (see Fig. S4), which seemed to contradict the result of Fig. 4A. We also explored whether the difference portrayed by Fig. 4A could be due to a different efficiency of CICR in both experimental types. To this end we performed stochastic puff simulations which indicated that the Ca^{2+}-mediated intra-cluster coupling is not different for Type I and III experiments (see Fig. S2).

Supplementary Fig. S4 related to this article can be found, in the online version, at http://dx.doi.org/10.1016/j.ceca.2015.01.003.

The contradictory results of the deterministic and stochastic simulations led us to explore how the different optical properties of Fluo-4 and of Rhod-2 affect the observed puff amplitude. To this end we applied the method introduced in [6] to obtain numerically generated images with realistic noise out of the noiseless simulations illustrated in Figs. S4 as described in Section 2.3.2. We recall that all the noiseless simulations were done with the same underlying Ca^{2+} source. We processed these numerically simulated images as done with the experimental ones and obtained the time profiles displayed in Fig. 5 A and B for Type I and for Type III, respectively. We show the spatial profiles in Fig. S5. In particular,
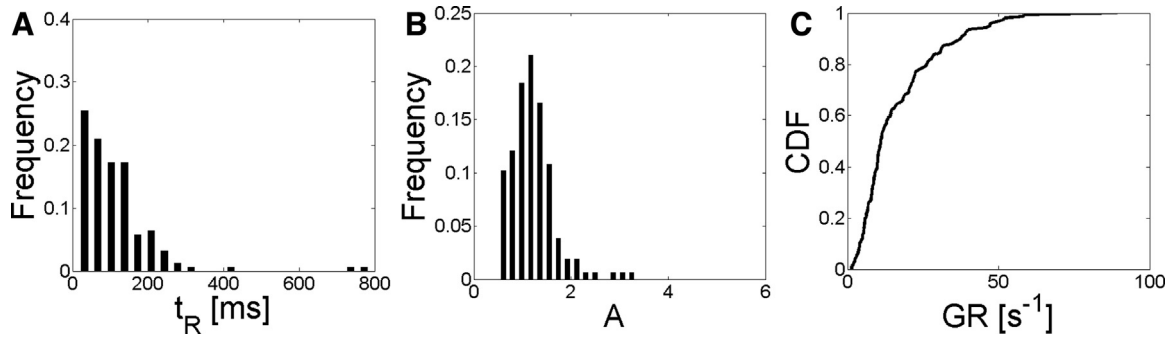
Fig. 3. Puff amplitude, rise-time and amplitude growth rate distributions for [Rhod2] = 90 μM and [EGTA] = 45 μM. Rise time (A), amplitude (B) and growth rate distributions (C) obtained from N = 157 puffs observed in Type III experiments. The mean rise time ($\langle t_R \rangle$) and standard deviations (σ_{t_R}) are $\langle t_R \rangle$ =111.6 ms and σ_{t_R} = 101.1 ms and the corresponding mean amplitude ($\langle A \rangle$) and standard deviations (σ_A) are $\langle A \rangle$ =1.2 au and σ_A = 0.5 au.
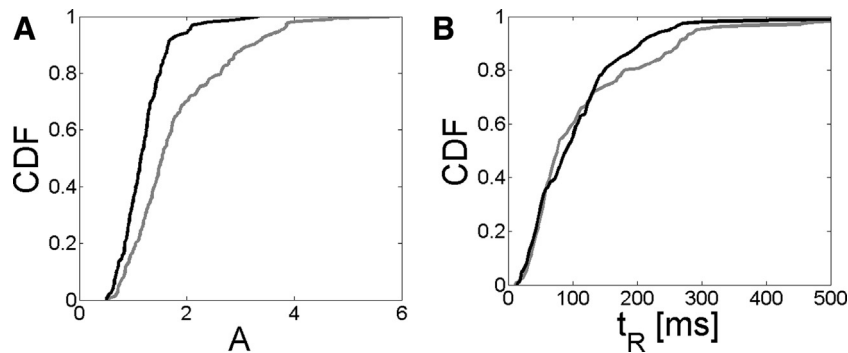

Fig. 4. Cumulative density functions. The cumulative density functions (CDF) of puff amplitude and rise time are plotted in (A) and (B), respectively, for type I (gray line) and Type III (black line) experiments. The CDFs were computed using the data displayed in Figs. 2A, 2C, 3A and 3B as explained in Section 2.2.2.

computing the width and decay time as explained in Section 2.3.2 we obtain Width = 0.9 μm, t_D = 54 ms for Type I and Width = 1.1 μm, t_D = 83 ms for Type III. We observe that t_D is larger for Type III than for Type I experiments, probably due to the different kinetics of Fluo-4 and Rhod-2. The amplitude, A (the maximum value of the temporal profile) is now smaller for Rhod-2 (A = 1.5) than for Fluo-4 (A = 2.3) which agrees with the experiments. This shows that having a method that generates images numerically with realistic noise is most important to compare experimental observations performed under different conditions.

Supplementary Fig. S5 related to this article can be found, in the online version, at http://dx.doi.org/10.1016/j.ceca.2015.01.003.

3.2.3. Large amplitude rapidly growing puffs are not observed in experiments performed with a slow dye and a relatively small [EGTA]

The simulations of Fig. 5 indicate that the (fluorescence) amplitudes of puffs that arise due to the same underlying Ca^{2+} current are smaller when observed with Type III than when observed with Type I experiments. The puff amplitude CDFs of Fig. 4A, however, cannot be transformed into one another by simply multiplying the amplitudes for one type of experiment by a constant factor. There is a long tail in the puff amplitude distribution of Fig. 2C that lacks in Fig. 3B. This different behavior also becomes clear in Table 3 where we list the average number of puffs observed per image when we
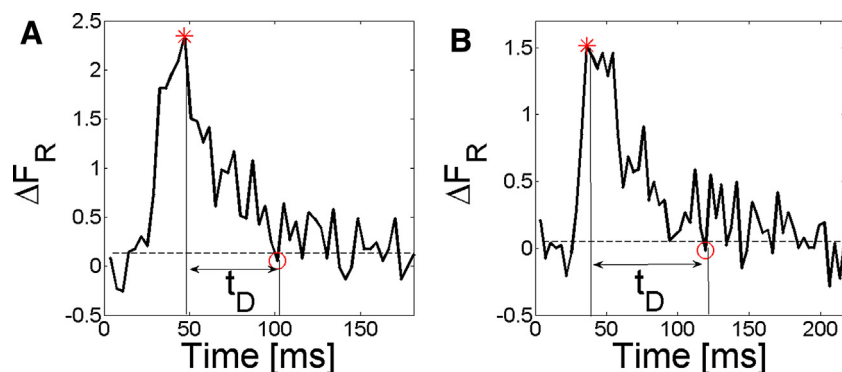
Fig. 5. Numerically simulated noisy profiles. Averaged temporal profiles for type I (A) and Type III experiments (B). We computed the amplitude and the decay time as with the experimental records obtaining A = 2.3, t_D = 54 ms for Type I and A = 1.5, t_D = 83 ms for Type III.
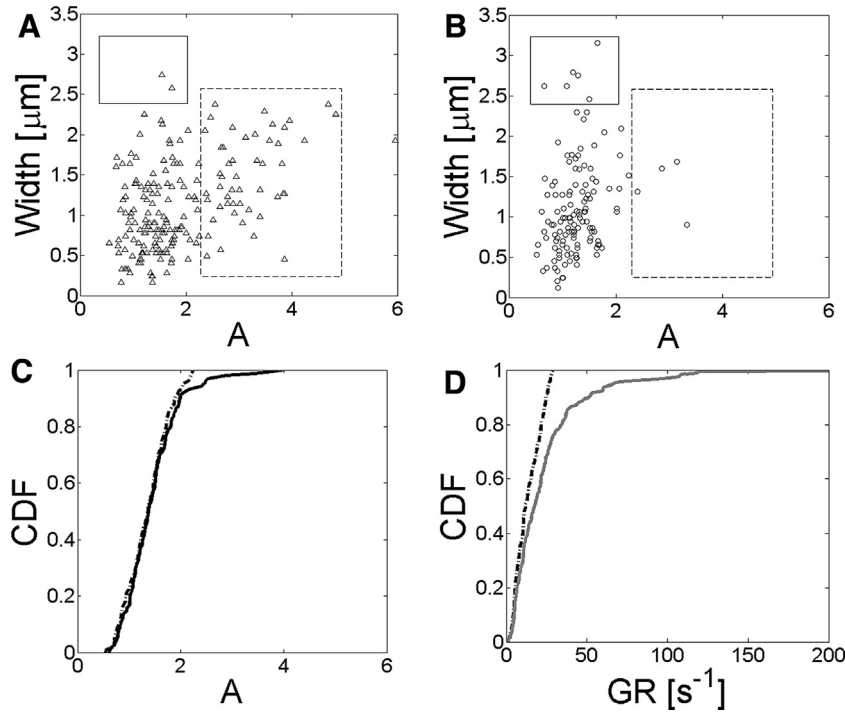
Fig. 6. Differences between the signals evoked in Type I and Type III experiments. (A) and (B) Scattered plot of width vs amplitude for the puffs observed in Type I (A) and Type III (B) experiments. Notice the different numbers of small amplitude wide puffs (in the regions enclosed with solid squares) and of large amplitude narrow puffs (in the regions enclosed with dashed squares) observed in both types of experiments. (C) Puff amplitude CDF of the subset with $A \leq 2.25$ of Type I experiments (dotted dashed line) and of all puffs observed in Type III experiments (black line), the latter with a conversion factor (1.2) in the amplitudes with respect to the ones determined from the images, $A_{new} = 1.2A_{old}$. (D) CDFs of amplitude growth rate obtained from Type I experiments when all the observed events (gray line) or the subset displayed in Fig. 6C (dotted dashed line) are kept.

limit the observations to puff amplitudes below a certain value. The differences in the distributions seem to indicate that different sets of Ca^{2+} release events are captured by Type I and Type III experiments. This hypothesis is reinforced by the observation that $\langle t_R \rangle$ is slightly smaller for Type III than for Type I although Rhod-2 has slower kinetics than Fluo-4. In order to probe the hypothesis we analyze now the observed puff distributions in terms of amplitude and width at the same time. We show the figures corresponding to puffs observed with Type I and Type III experiments in Fig. 6A and B, respectively. There we can see that puffs observed with Type III experiments are more stereotyped than those observed with Type I experiments. In particular, Type I experiments are able to detect puffs of relatively large amplitudes with almost any among the possible width values while the puffs of largest amplitude observed with Rhod-2 are not very wide (compare the regions surrounded by dashed line squares in Fig. 6A and B). Another difference is that some wide puffs with relatively small amplitudes are observed with Rhod-2 but are not reported in Type I experiments (see e.g., the regions indicated with solid squares in Fig. 6A and B).

In order to test if the different puff amplitude distributions obtained for Type I and Type III are due to a difference in the sets of events that are observed in both experimental types we computed the amplitude CDFs for a subset of events in the case of Type I. In order to compare this "restricted" CDF with the results of Type III experiments we used an amplitude conversion factor for the latter taking into account that, according to Fig. 5, the same source results in a signal with a smaller A for Type III with respect to Type I. If we compare Fig. 5A and B the conversion factor is about 1.5 (and it is 1.3 if we compare the spatial profiles shown in Fig. S5). We show in Fig. 6C the puff amplitude CDF of the subset with $A \leq 2.25$ of Type I experiments (dotted dashed line) and of all puffs observed in Type III experiments (black line), the latter with the conversion

factor, 1.2, in the amplitudes with respect to the ones determined from the images, $A_{new} = 1.2A_{old}$. We observe that these two CDFs are very much alike. The Kolomogorov test (Eq. (2)) does not reject, with a 5% significance level ($p_{value} = 0.803$), the null hypothesis that the amplitudes come from the same continuous distribution. If we compare the CDFs derived from all the events, the Kolmogorov test rejects the hypothesis that the data come from the same continuous distribution with a 5% significance level ($p_{value} = 3.6 \times 10^{-4}$). We show in Fig. 6D the CDFs of amplitude growth rate obtained from Type I experiments when all the observed events (gray line) or the subset displayed in Fig. 6C (dotted dashed line) are kept. We observe that the former includes events of larger growth rate than the latter. The Kolmogorov test rejects the hypothesis that the data come from the same continuous distribution with a 5% significance level ($p_{value} = 3.2 \times 10^{-5}$). We then conclude that, as in the case described in Section 3.1.1 the events that are captured by Type I experiments but are lost in Type III ones correspond to those with the largest growth rates.

4. Discussion

IP$_3$R-mediated Ca^{2+} signals are a key component of the Ca^{2+} signaling toolkit [3]. IP$_3$Rs are organized in clusters and their open probability depends on cytosolic Ca^{2+} [2]. Thus, the signals they mediate can remain spatially localized or propagate throughout the cell depending on the efficiency of CICR [14]. Local signals known as puffs [14] in which Ca^{2+} is released through IP$_3$Rs that belong to a single channel cluster are the building blocks of global signals [4]. Therefore, it is of great interest to understand their dynamics [12,15–19]. Ca^{2+} puffs are observed experimentally using single wavelength Ca^{2+} dyes and caged IP$_3$. To maximize the number of

observed events the slow buffer EGTA is usually added to prevent the CICR-mediated coupling between neighboring clusters [4,20].

In this paper we have combined imaging experiments and simulations to analyze how comparable the properties of puffs observed with different dyes and [EGTA] are and to what extent the elicited signals depend on the dye and [EGTA] used. To this end we have probed three experimental settings (see Table 1): Type I with a combination of dye and [EGTA] that has been proved to be adequate for the observation of Ca^{2+} puffs in *X. laevis* oocytes [18]; Type II with the same dye and concentration as in Type I but with larger [EGTA] and Type III with a dye of slower kinetics than the one used in Type I but at such a concentration and in combination with a value of [EGTA] for which the analysis of [6] shows that it should detect Ca^{2+} signals with a similar signal-to-noise ratio as Type I experiments. As discussed in what follows we conclude that the differences observed in the three types of experiments are due to the different degree of inter-cluster uncoupling. This is consistent with the fact that waves are observed much more frequently in Type III than in Type I and that signals that remain spatially restricted are practically not observed for experiments with [*Fluo*4] = 36 μM (as in Type I experiments) but [EGTA] = 45 μM (data not shown). Thus, even if different combinations of dye and EGTA allow, in principle, for the occurrence of puffs involving similar numbers of open IP_3Rs, different levels of inter-cluster coupling tailor differently the distributions of observed events. The analysis of the events that are missed in one or the other experiment type sheds light on the intra-cluster organization. We could readily compare the puff property distributions obtained in Type I and Type III experiments that use two dyes of very different kinetics because we have a classification method of experimental settings that allows us to generate numerical images of Ca^{2+} signals with realistic noise [6]. In this way we can separate the effect of the dye on the image, given a Ca^{2+} source, from its effect on the source itself through its modulation of CICR. The fact that the events that remain spatially localized in Type I and Type III experiments can be observed with similar accuracy in both cases proves the efficacy of our classification method. The possibility of applying the method to dyes that fluoresce in two different wavelengths such as Fluo-4 and Rhod-2, on the other hand, has an added value since ensuring comparability of puff properties observed with either one of them is necessary for a correct interpretation of experiments performed with both dyes simultaneously [21].

4.1. Comparison of puff properties obtained in the three types of experiments

We compared the distributions of puff amplitude and rise time of Type I and Type II (Fig. 2) and of Type I and Type III (Figs. 2A, 2C, 3A, 3B and 4) experiments. For the latter we also compared the distributions of puff width and decay time (Fig. S3). The corresponding Kolmogorov tests rejected the hypotheses that the data on rise time and on puff amplitude obtained for Type I and Type II experiments came from the same continuous distribution and that the data on puff amplitude and width obtained for Type I and Type III experiments came from the same continuous distribution both with a 5% significance level. The rest of the hypotheses were not rejected. According to the simulations presented in Fig. S3 and in Fig. 5, we could expect the same underlying Ca^{2+} release event to be portrayed with a different relative change in fluorescence amplitude for each experiment type. Thus, we explored if the puff amplitude distributions of Type I and Type II experiments matched each other after all the amplitudes observed in one of the experiment types were multiplied by a common factor. We found that this was indeed the case by multiplying the Type II amplitudes by 1.3 (see Fig. 2E). We performed a similar analysis to compare the puff amplitude distributions obtained for Type I and Type III

experiments. In this case we used the conversion factor 1.2 to multiply the amplitudes obtained in Type III. Even with this conversion factor the cumulative density functions differed considerably between both experiment types. The more detailed analysis of the event properties illustrated in Fig. 6A and B showed that the set of events observed in Type I and Type III experiments was apparently different. Namely, the events of largest amplitude observed in Type I were missing in Type III experiments. This observation was confirmed by a more quantitative comparison as shown in Fig. 6C. Namely, by keeping the subset with $A \leq 2.25$ for Type I experiments, the corresponding puff amplitude CDF matched the one obtained for Type III experiments using the conversion factor 1.2. Thus, we concluded that the set of events observable with Type I experiments embraced those that could be observed in Type III but also included other events of larger amplitude. Even though this is different from what we found in the comparison of Fig. 2E, Type I and Type II experiments also differ in the set of events that they detect. Namely, according to Fig. 2, the mean rise time was smaller for puffs observed in Type II than in Type I experiments. As we discuss in the next subsection the amplitude growth rate provides a unifying description of the events that are missed in one experiment type in comparison with another type.

4.2. The distributions of puff amplitude growth rate obtained for the different experiment types match each other after pruning the fastest growing events

The comparison of the amplitude growth rate ($GR = 0.9A/t_R$) displayed in Fig. 2F showed that the change in fluorescence was faster, on average, for Type II than for Type I experiments ($\langle GR \rangle_{II} = 30.2\,s^{-1}$ and $\langle GR \rangle_I = 24.7\,s^{-1}$). The Kolmogorov test applied to the CDFs of Fig. 2F rejects the null hypothesis that both data sets come from the same continuous distribution with a 6.1% significance level ($p_{value} = 0.061$). Even if this significance level is slightly worse than the standard value (5%), it is important to note that this result changes if only the subset with growth rates up to $100\,s^{-1}$ are kept to perform the comparison ($\langle GR \rangle_I = 21.1\,s^{-1}$ $\langle GR \rangle_{II} = 20.4\,s^{-1}$). In this case the Kolmogorov test cannot reject the null hypothesis and the p_{value} increases significantly (0.528). Thus, the set of events observable with Type II experiments embraces those that can be observed in Type I but also includes other events of faster amplitude growth rate. We then compared the amplitude growth rate distributions of Type I and Type III experiments. We found that if all the events were kept, the Kolmogorov test rejected the hypothesis that the data came from the same continuous distribution with a 5% significance level ($p_{value} = 4.0 \times 10^{-4}$). If we only kept the subset of events with $A \leq 2.25$ for Type I experiments, the corresponding growth rate CDFs matched each other. Again in this case the events that are "missed" in Type III experiments are those of fastest growth rate observed in Type I. As shown in Fig. S1 the faster growth rate for larger [EGTA] cannot be attributed to Ca^{2+} release from Ca^{2+}-bound dye or Ca^{2+}-bound EGTA. The stochastic simulations discussed in Fig. S2 also show that changing [EGTA] does not alter the intracluster coupling between IP_3Rs.

4.3. The three types of experiments differ in their ability to alter CICR between IP_3R clusters

The observation that different subsets of puffs are obtained in the three experiment types probed can be attributed to the different ways in which neighboring IP_3R clusters are effectively uncoupled in each type. We tested this possibility given the fact that waves are obtained more frequently in Type III than in Type I and in Type I than in Type II experiments (data not shown). The differences in inter-cluster coupling between the three types of experiments are illustrated in Fig. 7. There we show the probability, $P_O(d = 1.4\,\mu m,$
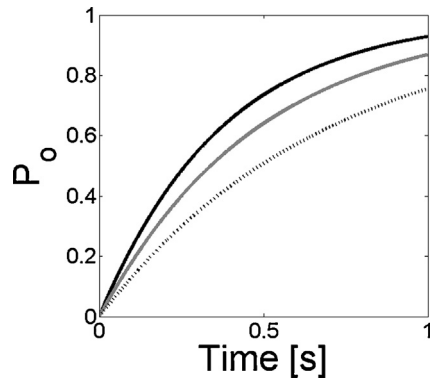
Fig. 7. Probability, $P(d, \Delta t)$, that an IP_3-bound IP_3R located at a distance d from a site of Ca^{2+} release opens before a time Δt has elapsed since the beginning of the release. We show the probability $P(d = 1.4\,\mu m, \Delta t)$ defined in Eq. (9), as a function of Δt for simulations performed under conditions mimicking those of Type I (gray line), Type II (dotted black line) and Type III (black line) in the presence of the same Ca^{2+} point source and using $[Ca^{2+}]_{basal} = 0.1\,\mu M$ for Type I, $[Ca^{2+}]_{basal} = 0.07\,\mu M$ for Type II and $[Ca^{2+}]_{basal} = 0.13\,\mu M$ for Type III experiments.

Δt), defined in Eq. (9), for simulations performed under conditions mimicking those of Type I (gray line), Type II (dotted black line) and Type III (black line) in the presence of the same Ca^{2+} point source. For the simulations we used $[Ca^{2+}]_{basal} = 0.1\,\mu M$ for Type I, $[Ca^{2+}]_{basal} = 0.07\,\mu M$ for Type II and $[Ca^{2+}]_{basal} = 0.13\,\mu M$ for Type III experiments. We repeated the simulations using $[Ca^{2+}]_{basal} = 0.1\,\mu M$ for Type II and III experiments, other values of d and a source involving more simultaneously open channels. In all cases we found the same trends but with different numbers. Namely, when comparing Type I and Type II experiments we obtain that the probability, $P_O(d, \Delta t)$, is smaller for Type II than for Type I experiments for all values of d, although the difference is maximal for $d \sim 1.4\,\mu m$ in the case of the source of Fig. 7. When comparing Type I and Type III experiments we obtain that $P_O(d, \Delta t)$ is smaller for Type III than for Type I experiments for d small enough. For distances above a minimum that depends on the source ($d \sim 0.4\,\mu m$ for the source of the figure) $P_O(d, \Delta t)$ is larger for Type III than for Type I experiments.

4.4. Different types of signals are evoked in the different types of experiments due to their different Ca^{2+} trapping capability

The differential Ca^{2+}-trapping capabilities at a distance from a release site of the three experiment types probed can explain the differences in the observed puff distributions. Namely, Ca^{2+} release events that involve the opening of many IP_3Rs in a cluster will be more likely to induce the opening of IP_3Rs in neighboring clusters in experiments with a less efficient Ca^{2+}-trapping capability at a distance in which case they would lead to a wave-like event and will not be included in our puff distributions. This can explain the absence of large amplitude narrow puffs in Type III as compared to Type I experiments displayed by Fig. 6A and B. The wide puffs of small amplitude observed in Type III but not in Type I experiments, also shown in these figures, could be related to out of focus puffs. Namely, such events would be more likely to be observable in experiments with less efficient Ca^{2+}-trapping such as those of Type III. The differences between the sets of puffs observed in Type I and Type II experiments can also be related to the more frequent occurrence of events involving the opening of more IP_3Rs in the latter than in the former. In this case the difference is reflected in the larger amplitude growth rate of the puffs observed in Type II when compared with Type I experiments (see Fig. 2F). In this case it is harder to observe the difference in terms of puff amplitude

because increasing EGTA has two opposite effects: that of allowing the observation of puffs that involve the simultaneous opening of more IP_3Rs and that of decreasing the Ca^{2+}-bound dye concentration and the relative increment in fluorescence. Furthermore, as shown in [7] the relationship between the relative increment in fluorescence and the maximum number of simultaneously open IP_3Rs is nonlinear, with puff amplitude growing slower than the number of open IP_3Rs. This nonlinearity is more acute the faster the underlying kinetics of the Ca^{2+} release process [7]. This reinforces the idea that the differences observed between Type I and Type II experiments can be attributed to the more frequent occurrence of puffs involving the opening of more IP_3Rs in Type II than in Type I experiments.

4.5. The different types of signals observed in the different types of experiments shed light on the architecture of IP_3R clusters in X. laevis oocytes

Figs. 2F and 6D show that both when comparing Type I with Type II or with Type III experiments the events that are missed in one or the other experimental type are those of the fastest amplitude growth rate in each case. In the previous subsections we have argued that the missing events correspond to those involving the largest Ca^{2+} release intensity. This implies that puffs involving the largest possible numbers of simultaneously open IP3Rs are also those with the fastest amplitude growth rate. This agrees with the observations of [22] obtained in SH-SY5Y cells in which the mean rise time remains approximately constant for puffs involving the opening of two or more IP_3Rs. It is also consistent with the analysis of [15] which led to the conclusion that the IP_3R clusters that underlie Ca^{2+} puffs in X. laevis oocytes do not show a large spatial size variability. This, in turn, implies that the larger the number of open IP_3Rs during a puff the smaller the mean distance between them. A smaller inter-channel distance, in turn, means a more efficient CICR at the intra-cluster level [16,23] and a faster amplitude growth rate [7]. This is different from assuming that IP_3-bound IP_3Rs are always separated by the same mean distance so that puffs of larger amplitude correspond to a larger cluster spatial size. The IP_3R cluster spatial extent has to be distinguished from puff width which reflects the region over which the [CaD] spreads. Having approximately the same cluster spatial extent is compatible with having an increasing spatial fluorescence width with increasing puff amplitude as observed in [22]. Namely, Ca^{2+}-trapping by buffers will be less efficient in the presence of a faster Ca^{2+} release which will result in [Ca^{2+}] and [CaD] spreading faster over a larger region in space.

Conflict of interest

None declared.

References

[1] A. Fabiato, Calcium-induced release of calcium from the cardiac sarcoplasmic reticulum, Am. J. Physiol. 245 (1983) C1–C14.

[2] J.K. Foskett, C. White, K.-H. Cheung, D.-O.D. Mak, Inositol trisphosphate receptor Ca^{2+} release channels, Physiol. Rev. 87 (2007) 593–658.

[3] C.-U. Choe, B.E. Ehrlich, The inositol 1,4,5-trisphosphate receptor (IP$_3$R) and its regulators: sometimes good and sometimes bad teamwork, Sci. STKE 2006 (2006) re15.

[4] J.S. Marchant, I. Parker, Role of elementary Ca^{2+} puffs in generating repetitive Ca^{2+} oscillations, EMBO J. 20 (2001) 65–76.

[5] R.M. Paredes, J.C. Etzler, L.T. Watts, W. Zheng, J.D. Lechleiter, Chemical calcium indicators, Methods 46 (2008) 143–151.

[6] E. Piegari, L. Lopez, E. Perez Ipiña, S. Ponce Dawson, Fluorescence fluctuations and equivalence classes of Ca^{2+} imaging experiments, PLoS ONE 9 (2014) e95860.

[7] G. Solovey, D. Fraiman, S. Ponce Dawson, Mean field strategies induce unrealistic nonlinearities in calcium puffs, Front. Physiol. (2011) 2.

[8] P. Cao, G. Donovan, M. Falcke, J. Sneyd, A stochastic model of calcium puffs based on single-channel data, Biophys. J. 105 (2013) 1133–1142.

[9] L. Sigaut, M. Barella, R. Espada, M.L. Ponce, S.P. Dawson, Custom-made modification of a commercial confocal microscope to photolyze caged compounds using the conventional illumination module and its application to the observation of inositol 1,4,5-trisphosphate-mediated calcium signals, J. Biomed. Opt. 16 (2011) 066013.

[10] G.W. De Young, J. Keizer, A single-pool inositol 1,4,5-trisphosphate-receptor-based model for agonist-stimulated oscillations in Ca^{2+} concentration, Proc. Natl. Acad. Sci. U. S. A. 89 (1992) 9895–9899.

[11] A.L. Escobar, P. Velez, A.M. Kim, F. Cifuentes, M. Fill, et al., Kinetic properties of DM-nitrophen and calcium indicators: rapid transient response to flash photolysis, Pflugers Arch. 434 (1997) 615–631.

[12] J. Shuai, H.J. Rose, I. Parker, The number and spatial distribution of IP$_3$ receptors underlying calcium puffs in *Xenopus* oocytes, Biophys. J. 91 (2006) 4033–4044.

[13] A. Minta, J.P. Kao, R.Y. Tsien, Fluorescent indicators for cytosolic calcium based on rhodamine and fluorescein chromophores, J. Biol. Chem. 264 (1989) 8171–8178.

[14] X.-P. Sun, N. Callamaras, J.S. Marchant, I. Parker, A continuum of InsP3-mediated elementary Ca^{2+} signalling events in *Xenopus* oocytes, J. Physiol. 509 (1998) 67–80.

[15] L. Bruno, G. Solovey, A.C. Ventura, S. Dargan, S.P. Dawson, Quantifying calcium fluxes underlying calcium puffs in *Xenopus laevis* oocytes, Cell Calcium 47 (2010) 273–286.

[16] G. Solovey, S.P. Dawson, Intra-cluster percolation of calcium signals, PLoS ONE 5 (2010) e8997.

[17] I.F. Smith, I. Parker, Imaging the quantal substructure of single IP$_3$R channel activity during Ca^{2+} puffs in intact mammalian cells, Proc. Natl. Acad. Sci. U. S. A. 106 (2009) 6404–6409.

[18] L. Lopez, E. Piegari, L. Sigaut, S. Ponce Dawson, Intracellular calcium signals display an avalanche-like behavior over multiple lengthscales, Front. Physiol. (2012) 3.

[19] D. Fraiman, S. Ponce Dawson, Buffer regulation of calcium puff sequences, Phys. Biol. 11 (2014) 016007.

[20] S.L. Dargan, B. Schwaller, I. Parker, Spatiotemporal patterning of IP3-mediated Ca^{2+} signals in *Xenopus* oocytes by Ca^{2+}-binding proteins, J. Physiol. 556 (2004) 447–461.

[21] E. Piegari, L. Lopez, L. Sigaut, S. Ponce Dawson, Studying calcium signal reshaping by buffers observing the competition of two dyes, Biophys. J. 102 (2012) 310a.

[22] D. Dickinson George, I. Parker, Factors determining the recruitment of inositol trisphosphate receptor channels during calcium puffs, Biophys. J. 105 (2013) 2474–2484.

[23] L. Diambra, J.S. Marchant, Inositol (1,4,5)-trisphosphate receptor microarchitecture shapes Ca^{2+} puff kinetics, Biophys. J. 100 (2011) 822–831.